

Novel Unsupervised Learning Architecture for Exposure-Based Classification and Enhancement

Mohit Kumar[✉] and Ashish Kumar Bhandari[✉]

Abstract—Numerous imaging applications are affected by the poor quality of images caused by poor illuminating conditions, contrast degradation, and unwanted noise. These effects create noticeable artifacts in an indeterministic selective manner, where some parts of the image are modified, and some parts of the image are uninfluenced. Thus, the classification of an image into various sections and, then, segmentwise application of imaging algorithms are a preferable solution. This article focuses on classifying an image into three categories as under-well-over exposed regions. This article introduces the concept of multilevel superpixel-based classification. Superpixel stores the local integrity and color similarity of an image; hence, an image is initially classified into an experimentally predetermined number of superpixels. Then, a novel algorithm depending upon the superpixel contrast, entropy, and statistical distribution of illumination classifies it into an under-well-over exposed region. Then, with an increased number of superpixels, we reiterate the whole process. The regions classified into the same category in both iterations perform as the training datasets for the support-vector-machine (SVM) classifier. Finally, the trained SVM classifies the ambiguous regions obtained from multilevel superpixel classification. Both qualitative and visual results show the superior performance of the proposed method over the state-of-the-art methods.

Impact Statement—Shadowing due to large nearby sculptures, improper illumination, backlighting with the subject in between the light source and camera, results in multi-exposed images. These images have a combination of well/under/over-exposed regions thereby effecting their visual quality. Classification of an image into these three regions helps to selectively apply different artificial intelligence (AI) based image processing algorithm to get desired result. We also show the application of the proposed classification algorithm in extracting hidden information from an image thereby improving the visual aesthetic of the image. A well classified image can help to boost the visibility of dark regions assisting AI based self-driving cars in night-time, enhance selective regions of a medical image to improve diagnosis with AI, and can help to improve the feature selection in biometric recognition systems. The paper proposes a novel pipeline to adaptively classify an image into multi-level superpixels. An algorithm is designed to use the

Manuscript received 11 February 2022; revised 12 May 2022; accepted 1 July 2022. Date of publication 12 July 2022; date of current version 22 September 2023. This paper was recommended for publication by Associate Editor B. Xue upon evaluation of the reviewers' comments. (*Corresponding author: Ashish Kumar Bhandari*.)

Mohit Kumar is with the Department of Electronics and Communication Engineering, National Institute of Technology, Patna 800005, India, and also with the Muzaffarpur Institute of Technology, Muzaffarpur 842003, India (e-mail: engg.mohitkumar@gmail.com).

Ashish Kumar Bhandari is with the Department of Electronics and Communication Engineering, National Institute of Technology, Patna 800005, India (e-mail: bhandari.iiitj@gmail.com).

Digital Object Identifier 10.1109/TAI.2022.3190240

properties of the superpixels to both train and test a multi-class support-vector-machine without any need of a supervised learning.

Index Terms—Image classification, image enhancement, multilevel superpixel, support-vector-machine (SVM).

I. INTRODUCTION

OOD quality of an image is an utmost requirement for many image processing algorithms. It helps in proper image enhancement, segmentation, feature extraction, matching, classification, compression, and numerous other operations [1], [2]. The regions of an image presenting clear perceptual information are termed well-exposed regions, whereas those with complete/partial loss of visual information are classified as under/overexposed regions. Nonuniform illumination due to different lighting conditions results in a similar intensity of both background and region of interest. Thus, the classification of an image based on image intensity only creates erroneous results. This limitation has encouraged researchers to use different properties of an image namely contrast and entropy along with the intensity for proper classification of an image [3]–[17]. Contrast enhancement methods that apply the same rate of enhancement for both dark (underexposed) and bright (overexposed) regions often result in the loss of information in the bright regions. This problem overcomes by predetermining the exposure characteristics of different regions of an image and applying variable enhancement rates for different zones [13], [14]. These developments in recent research have motivated us to design an unsupervised learning architecture to classify an image into three different exposure zones and design different enhancement rates for each of the zones.

Classification acts as a preprocessing step in many image processing algorithms [3]. One of the primary uses is in the contrast enhancement of an image. An image is enhanced in [4] by first decomposing it into color similarity constrained reflectance and piecewise smoothness constrained illumination component and then adjusting the illumination layer. A segmentation-based approximation of the Milano Retinex model utilizes the relevant color and spatial information obtained by image classification to obtain enhancement [5]. Transformation in the dark and bright regions is separately modified in [6] using an optimum threshold value obtained using the Salp–Swarm algorithm. However, the performance of these methods in low-light images was not satisfactory [7]. An objective measure termed exposure has been

formulated in [8] to demarcate over and underexposed regions. Sigmoid function improves the luminance of the underexposed region, whereas a power-law operator improves the overexposed region. Hasikin and Isa [9] divide a degraded image into the bright and dark regions using a novel coined parameter “contrast factor.” Then, a modified Gaussian membership function with fuzzy set theory enhances poorly illuminated images. A high dynamic range color image classification into underexposed, mixed-exposed, and overexposed regions is done in [10]. Here, the authors use the Shannon entropy function, and a visual appeal indicator is modified using ant colony optimization to achieve an enhanced image. Lee *et al.* [11] partitioned an input image using fuzzy logic into a dark object and bright background regions. The authors tested their method majorly on backlit images and performed contrast stretching in the dark region. Saad *et al.* [12] used the local neighborhood image properties for exposure region detection (LNIERD) to demarcate images in three exposed categories of under-well-over exposed regions. The nonlinear exposure intensity-based modification histogram equalization in [13] divides the well-exposed region again into three more regions and obtains an enhanced image by modifying the cumulative distribution function of each region’s histogram. An entropy-controlled gray level distribution is done and the image is repartitioned using new threshold values before histogram equalization in [14]. In medical image processing [15], irregular mass is first segmented from the wavelet decomposed image and then a different enhancement algorithm is applied to the foreground and background to identify the disease. Prabukumar [16] and Clement and Baskar [17] have done contrast enhancement by doing modifications in discrete wavelet and discrete cosine domain, respectively. In [16], at first, local contrast of an image in the hue, saturation and value (HSV) domain is enhanced by modifying the discrete wavelet transform (DWT) coefficients, thereby saturation component is histogram equalized to obtain global enhancement as well. The use of superpixel to divide a breast ultrasound image into numerous parts, which train a convolutional neural network to enhance and determine the status of the tumor, is proposed in [18].

Haze removal techniques aim to improve the reflected light from mixed light, so, inherently, most of the Retinex-based methods use classification. Pixelwise weight maps depending on both local and global exposedness are obtained from underexposed images. These maps then guide a fusion process to dehaze the image [19]. Berman *et al.* [20] considered multiple spectral profiles of different water types and estimated attenuation ratio of blue-red and blue-green color channels to reduce the underwater enhancement problem as an image dehazing problem. Atmospheric light is estimated in [21] using a support-vector-machine (SVM) classifier from the classified sky region; a multiscale opening dark channel model does the work of haze removal. Apart from these, the classification of an image finds its application in numerous other image processing domains, such as reconstruction of the indoor scene [22], classification of fine-grained food [23], multioriented text detection [24], and perceptually invisible image enhancement [25], [26].

The main contribution and novelty of the proposed algorithm are as follows.

- 1) An unsupervised novel multilevel superpixel algorithm is proposed to classify an image into an optimum number of patches.
- 2) A classification algorithm is designed that utilizes the exposure, contrast, and intensity value of a superpixel to categorize it as an under-well-over exposed region. The statistical properties, namely mean standard deviation and kurtosis, are utilized to obtain optimum threshold values for the classification.
- 3) A pipeline is proposed to generate both training and testing datasets from the same image to train and test a multiclass SVM. The unsupervised nature of the learning helps to improve the overall classification accuracy.
- 4) A new enhancement algorithm that utilizes different enhancement rates for different exposed zones is conceptually designed to validate the real-life application of the proposed method. The proposed architecture successfully enhances the images suffering from multiple exposure regions and brings out perceptually invisible available information. Many of the state-of-the-art enhancement algorithms fail to enhance these images.

The rest of this article is as follows. In Section II, we explain our novel proposed methodology of a multilevel superpixel-based multiclass SVM classifier. We follow this with thorough quantitative and visual analysis in Section III. Section IV explains an application of the proposed algorithm using a novel enhancement algorithm. Finally, Section V concludes this article.

II. PROPOSED CLASSIFICATION METHODOLOGY

An image is categorized into under-, well-, and overexposed regions. Well-exposed regions appear visually pleasing and need no further enhancement. In contrast, underexposed regions have hidden information in them and are visually imperceptible due to insufficient illumination. Finally, regions with high-intensity zones leading to a loss of contrast and vital information are termed overexposed regions. This article intends to classify an image into three different regions. The pipeline of the proposed algorithm is presented in Fig. 1. Initially, an image is classified into experimentally determined α -superpixel regions and β -superpixel regions using a novel designed multilevel superpixel algorithm (yellow box). Each of these regions based on their local characteristics is classified as an under-, well-, or overexposed region (green box). So, a particular region of an image is classified two times. Once when it is a part of α -superpixel classification and, second, when it is a part of β -superpixel classification. A confusion matrix is created from the obtained result. If the same region of the image is classified into the same category (under/well/over), then it will act as a training set of our proposed unsupervised multiclass SVM. However, if the same region of the image is classified as one category (e.g., under) in α -superpixel classification and into any other category (e.g., well/over) in β -superpixel classification,

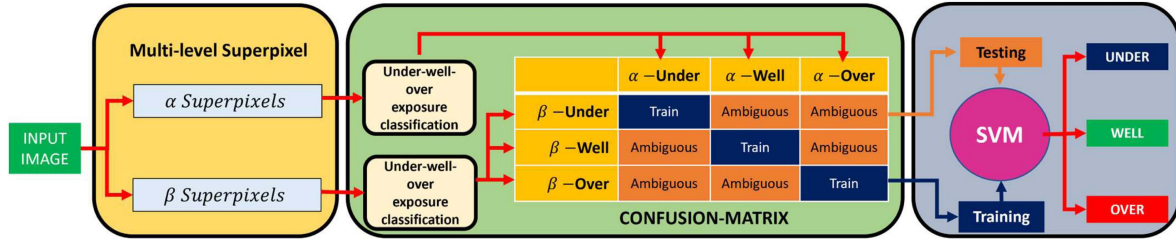


Fig. 1. Method pipeline: the proposed algorithm is categorized into three main categories. (a) Multilevel superpixel-based patch creation (yellow box). (b) Contrast, entropy, and statistical distribution of illumination-based under-well-over exposed superpixel region classification (green box). (c) Multiclass SVM training and testing to classify image into under-well-over exposed region (blue box).

then it will form a part of a testing dataset. Multiclass SVM is trained and tested on the classified superpixel region to achieve the final classification (blue box).

A. Multilevel Superpixel Algorithm

This section aims to segment an input image of size $M \times N$ into smaller patches. The size and boundary of patches should be flexible enough to encompass local structural attributes, similar color composition, and identical mutual information between neighboring pixels. To accumulate pixels of similar characteristics, we employ simple linear iterative clustering (SLIC) algorithm to create superpixels. A five-dimensional $[labxy]$ space is used, which was developed by the Commission of Illumination with pixel coordinate $[xy]$ vector and color space vector $[lab]$, where l represents the lightness, and a and b represent the chromaticity [27]. Two objective functions namely color similarity and proximity of pixels in $[xy]$ plane is optimized to cluster the pixels into superpixels. A modified distance measure between center pixels $[l_p, a_p, b_p, x_p, y_p]$ and each pixel $[l_i, a_i, b_i, x_i, y_i]$ is computed using (1). Euclidean distance in $[lab]$ space and $[xy]$ domain obtained using (2) and (3) signify spatial proximity and color similarity between the center pixel and the considered pixel

$$D_{\text{PIXEL}} = D_{\text{lab}} + \frac{m}{G} D_{xy} \quad (1)$$

$$D_{\text{lab}} = \sqrt{(l_p - l_i)^2 + (a_p - a_i)^2 + (b_p - b_i)^2} \quad (2)$$

$$D_{xy} = \sqrt{(x_p - x_i)^2 + (y_p - y_i)^2} \quad (3)$$

where m represents the contribution of spatial components, and G is the total number of pixels in the considered superpixel. SLIC dynamically normalizes the proximities for each cluster using its maximum observed spatial and color distances from the previous iteration. The algorithm keeps track of the maximum distance for each cluster and updates the value of m at each iteration. Based on the obtained D_{PIXEL} value, cluster center and associated pixels are updated till the attainment of convergence.

The number of superpixels into which an image should be divided for proper classification varies from image to image. If the number is too high, the size of each superpixel becomes very low, thereby increasing the computational complexity. On the other hand, if we reduce the number of superpixels beyond a particular limit, tracing and demarcation of boundary regions

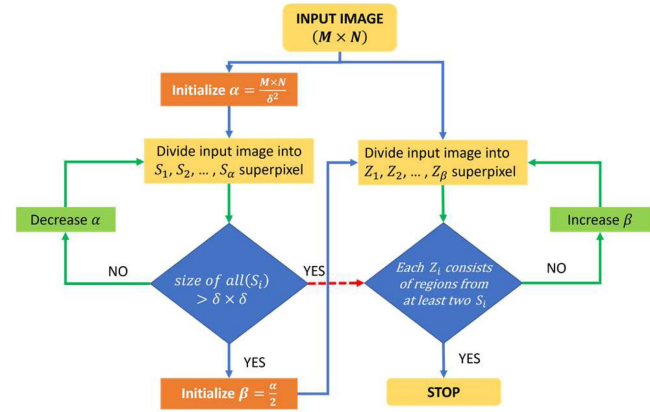


Fig. 2. Flowchart of the multilevel superpixel-based patch creation algorithm. Here, $M \times N$ represents the size of the input image and δ is the time-complexity parameter.

Algorithm 1: Exposure-Based Classification.

```

1: Compute  $E_{\text{IMAGE}}$  and  $C_{\text{IMAGE}}$            ← (5, 7)
2: Repeat
3:   Compute  $E_{\text{SP}}$  and  $C_{\text{SP}}$              ← (4, 6)
4:   if  $E_{\text{SP}} > E_{\text{IMAGE}}$  &&  $C_{\text{SP}} > C_{\text{IMAGE}}$ 
5:     Assign: Well-exposed superpixel
6:   else
7:     Compute  $T_{\text{LOW}}$  and  $T_{\text{HIGH}}$       ← (15, 16)
8:     Compute  $V_{\text{SP}}$                   ← (14)
9:     if  $V_{\text{SP}} < T_{\text{LOW}}$ 
10:       Assign: Underexposed superpixel
11:     elseif  $T_{\text{LOW}} < V_{\text{SP}} < T_{\text{HIGH}}$ 
12:       Assign: Well-exposed superpixel
13:     else
14:       Assign: Overexposed superpixel
15:     end if
16:   end if
17: until  $\{S_1, S_2, \dots, S_\alpha\}$  and  $\{Z_1, Z_2, \dots, Z_\beta\}$ .

```

become unacceptable. Also, the accuracy of classification based on the noniterative superpixel is not high. So, to solve these problems, we propose a novel multilevel superpixel-based patch creation algorithm (see Fig. 2).

Our algorithm is initialized by dividing the image of size $M \times N$ into α -superpixels using SLIC algorithm [27]. The initial

value of α is obtained by dividing the total number of pixels in an image by the square of the time-complexity parameter δ , which is obtained experimentally (see Section IV-D). As we increase the value of δ , the number of superpixels and, thereby, the computation time complexity decreases. In the first step, the image is divided into α superpixel, $\{S_1, S_2, \dots, S_\alpha\}$. The SLIC algorithm tries to classify the image while preserving the boundary between different regions of an image. This results in some superpixels with very large size and some with very small size. If the size of any superpixel is less than $\delta \times \delta$, then the value of α is decreased from the previous value and a new set of larger superpixel is obtained. The same process is iterated until all the superpixels S_i have a size greater than $\delta \times \delta$. Once the value of α is obtained, β is initialized as half of the final value of α . The image is again divided into β superpixel, $\{Z_1, Z_2, \dots, Z_\beta\}$. The size of each of these Z_i superpixel is more than previously classified S_i superpixel. A size criterion is imposed on these Z_i superpixels so that we can train our unsupervised multiclass SVM successfully. If each of these Z_i superpixel consists of the regions with at least two S_i superpixels, then only the algorithm is stopped and the final value of β is obtained. The value of β is increased by one at each iteration till the size criterion is satisfied.

B. Exposure-Based Classification Algorithm

An image is a conglomeration of smaller units called pixels. Classification of an image into different regions based on only each pixel intensity value does not weigh local characteristics. Thus, here, we propose a novel algorithm based on the concepts formulated in [12] that utilizes intensity distribution, contrast, and entropy of the local region. Algorithm 1 represents the flow to classify the superpixel into an under-well-over exposed category. The classification problem depends upon three parameters, the intensity value obtained from the HSV representation of the image, and the entropy and contrast obtained from the gray counterpart of the image. A superpixel with high contrast and high entropy represents the presence of information, so irrespective of its intensity value, it will be classified as a well-exposed region. However, if either entropy or contrast of a region is low, we cannot certify the presence or absence of information with certainty. In such cases, superpixel is dependent on its intensity-based classification.

1) *Entropy and Contrast-Based Classification:* Entropy and contrast-based classification help to extract regions with concealed information in either highly dark or bright areas. If the entropy [29] of the superpixel E_{SP} (4) exceeds the average entropy value of the whole image E_{IMAGE} (5), then the region is classified in the high entropy zone and vice-versa. Similarly, if the contrast [30] of the superpixel C_{SP} (6) exceeds the average contrast value of the whole image C_{IMAGE} (7) the region is classified to be in the high contrast zone

$$E_{SP} = - \sum_{i=0}^{2^n-1} p_i \log_2 p_i \quad (4)$$

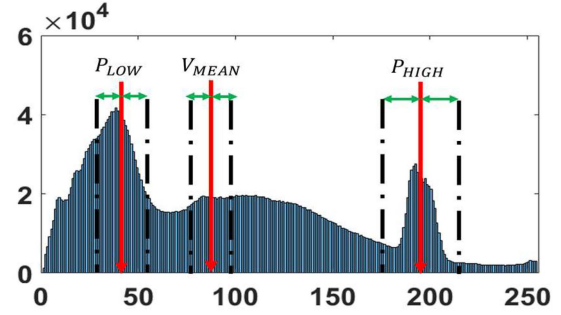


Fig. 3. Histogram of image representing mean value of image, lower half and upper half peaks, and their corresponding standard deviations.

$$E_{IMAGE} = \frac{1}{\alpha} \sum_{j=1}^{\alpha} E_{SP}(j) \quad (5)$$

$$C_{SP} = \frac{\alpha}{M \times N} \sum_{i=1}^{M/\alpha} \sum_{j=1}^{N/\alpha} G^2(i, j) - \left| \frac{\alpha}{M \times N} \sum_{i=1}^{M/\alpha} \sum_{j=1}^{N/\alpha} G(i, j) \right|^2 \quad (6)$$

$$C_{IMAGE} = \frac{1}{\alpha} \sum_{j=1}^{\alpha} C_{SP}(j) \quad (7)$$

where p_i is the probability of a gray level, and for proper computation, and a minimum 3×3 block size with eight neighboring cells is mandatory to account for variations in all possible directions. α is the number of superpixels obtained in the image of size $M \times N$. Hence, the size of each superpixel is approximately $\frac{M \times N}{\alpha}$. $G(i, j)$ represents the image's gray level at the location of (i, j) .

2) *Intensity-Based Classification:* The value constituent in HSV space determines the brightness component of the image. The lower and upper threshold values are obtained based on the statistical characteristics of the histogram of an image. For a gray image of size $M \times N$, we divide the image histogram $H(x)$ into two halves based on the mean value of the image V_{MEAN} (8). Then, two highest peaks, one in the lower half P_{LOW} and one in the upper half P_{HIGH} , are obtained (9). The distribution around each peak is analyzed separately with the help of Kurtosis (10). A normal distribution has a value of Kurtosis as three [31]. If the value of Kurtosis is more than three, it signifies a leptokurtic curve with a sharper central peak and longer tails, as represented by the peak in the upper half of Fig. 3. A negative kurtosis value signify platykurtic distribution with broader peak and shorter tails [31], as visible in the lower half peak of Fig. 3

$$V_{MEAN} = \frac{1}{M \times N} \sum_{i=1}^M \sum_{j=1}^N V(i, j) \quad (8)$$

Peak

$$= \begin{cases} P_{\text{Low}} = x \ni \max \{H(x) : x \in \mathbb{Z} \wedge 1 \leq x \leq V_{\text{MEAN}} - 1\} \\ P_{\text{High}} = x \ni \max \{H(x) : x \in \mathbb{Z} \wedge V_{\text{MEAN}} \leq x \leq 2^n - 1\} \end{cases} \quad (9)$$

where $H(x)$ represents the histogram of an n -bit image with intensity values between 0 and $2^n - 1$.

$$k = \begin{cases} k_{\text{Low}} = \frac{\sum_{i=0}^{V_{\text{MEAN}}-1} (i - P_{\text{Low}})^4}{\left(\frac{\sum_{i=0}^{V_{\text{MEAN}}-1} (i - P_{\text{Low}})^2}{V_{\text{MEAN}}} \right)^2} \\ k_{\text{High}} = \frac{\sum_{i=V_{\text{MEAN}}}^{2^n-1} (i - P_{\text{High}})^4}{\left(\frac{\sum_{i=V_{\text{MEAN}}}^{2^n-1} (i - P_{\text{High}})^2}{V_{\text{MEAN}}} \right)^2}. \end{cases} \quad (10)$$

Three standard deviations are calculated (see Fig. 3), first for the whole image (11), second for the lower half peak (12), and third for the upper half peak (13). In (11), since we are considering only the lower half, so instead of dividing the sum by the total size of the image, we divide it by the number of pixels having a value less than V_{MEAN} , which we obtain from the histogram of the image. Also, as we are interested in distribution about the peak, the standard deviation calculation takes place around P_{Low} in place of the mean of image. A similar procedure computes the standard deviation around P_{High} in (13)

$$\sigma_{\text{IMAGE}} = \sqrt{\frac{1}{M \times N} \sum_{i=1}^M \sum_{j=1}^N (V(i, j) - V_{\text{MEAN}})^2} \quad (11)$$

$$\sigma_{\text{Low}} = \sqrt{\frac{1}{\sum_{k=1}^{V_{\text{MEAN}}-1} k H(k)} \sum_{i=1}^M \sum_{j=1}^N (V(i, j) - P_{\text{Low}})^2} \quad (12)$$

$$\sigma_{\text{High}} = \sqrt{\frac{1}{\sum_{k=V_{\text{MEAN}}}^{2^n-1} k H(k)} \sum_{i=1}^M \sum_{j=1}^N (V(i, j) - P_{\text{High}})^2}. \quad (13)$$

A superpixel of size $a \times b$ is classified as underexposed if its value component V_{SP} (14) is smaller than the lower threshold value T_{Low} (15). If the value component is greater than the upper threshold value T_{High} (16), then it is classified as overexposed, and for all other cases, it is well-exposed superpixel (Algorithm 1).

$$V_{\text{SP}} = \frac{1}{a \times b} \sum_{i=1}^a \sum_{j=1}^b V(i, j). \quad (14)$$

Fig. 4 represents the flowchart of the method, which is used to compute the lower and upper threshold values. The threshold value of an image is obtained based on the nature of its histogram. If an image is well-exposed, then its distribution will be centered around its mean value. The distribution around P_{Low} and P_{High} in this case will be nearly flat with the kurtosis value k_{Low} and k_{High} less than three. Thus, here, lower threshold value will be the difference between the mean value and the standard deviation of the image (15), and the upper threshold value will be the

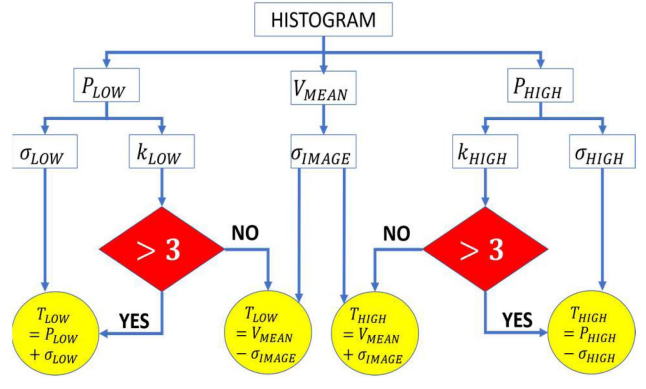


Fig. 4. Flowchart to compute low and high threshold based upon *Value* component of HSV image.

addition of the same (16). In the case of an image with a dominant underexposed region, we will find a peak in the lower half and k_{Low} will be more than three. Here, the lower threshold value will be obtained as the sum of the location of the lower peak and the standard deviation around it (15). Similarly, for an image with a dominant overexposed region, there will be a peak in the upper half of the histogram with k_{High} more than three. Here, the higher threshold value will be the sum of the location of the upper peak and the standard deviation around it (16). A normal distribution has a kurtosis value $k = 3$ and is known as mesokurtic. A distribution with a kurtosis value greater than normal distribution signifies that high variance in the distribution is due to infrequent extreme deviation. So, to account for these deviations, we propose that the threshold values in these cases should depend upon the distributions' peak value. However, if there is a platykurtic distribution around the peaks with a kurtosis value lower than three, the threshold values are obtained around the mean value of the whole image.

$$T_{\text{Low}} = \begin{cases} P_{\text{Low}} + \sigma_{\text{Low}}, & \text{where } k_{\text{Low}} \geq 3 \\ V_{\text{MEAN}} - \sigma_{\text{IMAGE}}, & \text{where } k_{\text{Low}} < 3 \end{cases} \quad (15)$$

$$T_{\text{High}} = \begin{cases} P_{\text{High}} - \sigma_{\text{High}}, & \text{where } k_{\text{High}} \geq 3 \\ V_{\text{MEAN}} + \sigma_{\text{IMAGE}}, & \text{where } k_{\text{High}} < 3 \end{cases}. \quad (16)$$

C. Multiclass SVM

SVM mathematically tries to optimize

$$\min_{w, b, \zeta} \frac{1}{2} w^T w + C \sum_{i=1}^n \zeta_i \quad (17)$$

$$y_i (w^T \phi(x_i) + b) \geq 1 - \zeta_i \quad (18)$$

$$w = \sum_{j=1}^N \alpha_j y_j \phi(x_j) \quad (19)$$

$$\phi(x_i, x_j) = \phi(x_i) \cdot \phi(x_j) = e^{-\gamma x_i \cdot x_j^2} \quad (20)$$

where y_i denotes the i th target value, $w^T w$ represents the normal vector, b denotes a bias parameter, and $\phi(x_i)$ is the transformed input vector using radial basis kernel. From (20),

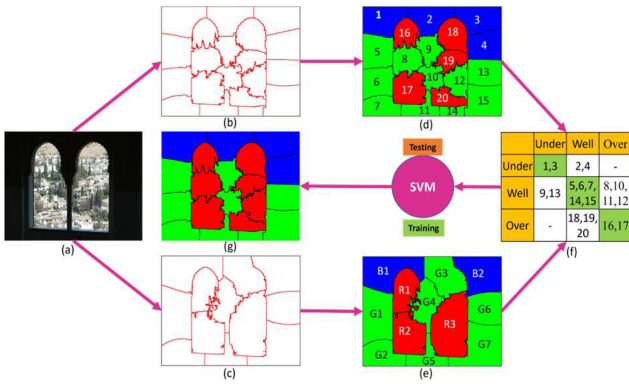


Fig. 5. Explanation of the proposed algorithm on the *Window* image, (a) input image, (b) SLIC-based classification of image into $\alpha = 20$ superpixels, and (c) SLIC-based classification of image into $\beta = 12$ superpixels. The values of α and β are kept very low for proper visualization and explanation purpose only. (d) and (e) Classification of superpixels into under-well-over exposed region based on flowchart Algorithm 1. (f) Confusion matrix with training and ambiguous testing data. (g) Multiclass SVM classified final output image.

one can observe that the kernel function ϕ can be written as the dot product of two terms $\phi(x_i)$ and $\phi(x_j)$. Now, $\phi(x_j)$ is further modified using (19) to obtain w , which is transposed and used in (18) and (21). The aim is to find optimal w and b to improve prediction accuracy [32]. But all data points are not correctly predicted, so a distance term to correct the margin ζ_i is introduced. For practical scenarios, a penalty term in the minimization formulae controlled by a regularization parameter C is induced. The double optimization problem of maximizing the margin while minimizing the parameters can be solved using Lagrange multipliers, where $a = (\alpha_1, \dots, \alpha_N)^T$.

$$L(w, b, a) = \frac{1}{2} w^2 - \sum_{n=1}^N a_n \{y_n (w^T \phi(x_n) + b) - 1\}. \quad (21)$$

Solving this optimization problem, we can classify new data points using

$$\sum_{n=1}^N \alpha_n y_n \phi(x_i, x_j) + b \quad (22)$$

where $\phi(x_i, x_j)$ corresponds to the transformed input vector using radial basis kernel on a single data point in the testing dataset and α_n and y_n are the learned N -dimensional vectors obtained after the training of the SVM.

1) *Problem Statement:* Multilevel classification may lead to the classification of the same region into different categories. This classification issue is perceptible in our example as well. Regions “2 and 18” earlier classified as underexposed (blue) and overexposed (red) superpixels [see Fig. 5(d)] are partially classified as well-exposed region G3 (green) in the new classification [see Fig. 5(e)]. A multiclass SVM [33] trained and tested on the multilevel classified image solves this ambiguity and improves classification accuracy.

2) *Multiclass Classification Algorithm:* Comparison of the classification output of multilevel superpixels generates a confusion matrix. The value of α is greater than β , as β satisfies the constraint that there must be at least two superpixels in any

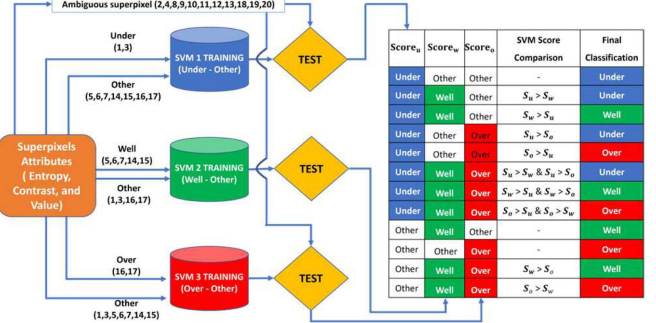


Fig. 6. Flowchart of the training and testing of the multiclass SVM algorithm. For explanation purpose, the numbers in the bracket are the classified superpixels form the confusion matrix [see Fig. 5(f)].

region covered by a single α classified superpixel. So, the size of α classified superpixels will be smaller than that of β classified superpixels. If a region in an α classified superpixel has the same category in β classified superpixel, we can be convinced about its accuracy. The characteristics, namely mean intensity value, contrast, and entropy, of such regions will act as input training feature vector for the SVM. In the considered example from Fig. 5(d) and (e), we can observe that α superpixel regions “1 and 3” are classified as underexposed in both cases. Similarly, regions “5, 6, 7, 14, and 15” are classified as well exposed, and “16 and 17” are classified as overexposed in both cases. However, some regions are classified into different categories in both scenarios. So, there arises an ambiguity in such cases about the exact nature of such superpixels. In Fig. 5(d), regions “9 and 13” are classified as well exposed in α superpixel case. However, these regions are partially classified as well exposed and partially underexposed in Fig. 5(e). Such ambiguous regions’ properties act as testing feature vector for the SVM. The accumulation of these cases and training dataset completes the confusion matrix, which will be unique for each image [see Fig. 5(f)]. The SVM trained and tested on the feature vector generated from the regions of this confusion matrix gives our final classified output as Fig. 5(g). Fig. 6 summarizes the multiclass SVM designed to classify a superpixel as under/well/overexposed region. At first, we find the entropy, contrast, and mean value of each superpixel. We train three SVM classifiers using the information from the confusion matrix [see Fig. 5(f)]. All these three SVMs are trained using the attributes of those superpixels only, which are classified into the same category during both α - and β -based classification [regions 1, 3, 5, 6, 7, 14, 15, 16, and 17 in Fig. 5(d)]. SVM-1 is trained to classify any superpixel as either underexposed region or not-underexposed (other) region. Similarly, SVM-2 classifies any superpixel as either well-exposed region or not-well-exposed (other) region and SVM-3 classifies any superpixel as either overexposed region or not-overexposed (other) region. Then, an ambiguous region’s [2, 4, 8, 9, 10, 11, 12, 13, 18, 19, and 20 in Fig. 5(f)] attribute is given as a testing data to each of the classifier and their output and classification confidence score are recorded. Finally, the superpixel is classified into its relevant category based on the comparison of the confidence score of the three SVM’s output (table in Fig. 6). In the output

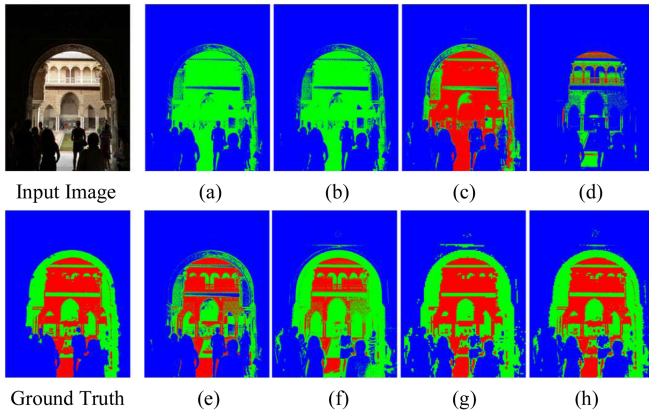


Fig. 7. Visual comparision of the *Monument* image. The results of different techniques are viz., (a) exposure 2R [8], (b) contrast factor [9], (c) exposure 3R [10], (d) LEI-ANN [36], (e) ICEVE [37], (f) BACKLIT [11], (g) LNIERD [12], and (h) proposed method.

[see Fig. 5(g)], we can observe the impact of training on a few regions, as the regions “8 and 12” earlier classified as a well-exposed region are now classified as an overexposed region.

III. EXPERIMENTAL RESULT ANALYSIS

We justify the proposed algorithm’s superior performance by evaluating and comparing its performance in both the classification and real-life application domains. We will also analyze the enhancement algorithm, which uses the classification outcome to support the algorithm’s application potentiality. The algorithm is tested on 524 images across the Berkley Segmentation Dataset (BSDS) [34] and the Vasileios Vonikakis (VV) dataset [35]. All the quantitative and qualitative analyses are done with respect to the seven state-of-the-art methods, namely exposure 2R [8], contrast factor [9], exposure 3R [10], low exposure image using artificial neural network (LEI-ANN) [36], image enhancement using classified virtual exposure [37], BACKLIT image enhancement method [11], and local neighborhood image properties for exposure region determination (LNIERD) [12].

A. Visual Analysis of Classification

From the visual analysis, we can see that the exposure 2R and contrast factor classify all the images either in under- or well-exposed regions. In Fig. 7, exposure 3R classifies many well-exposed pixels into overexposed pixels, whereas LEI-ANN classifies them into underexposed pixels. The output from the ICEVE, BACKLIT, and the proposed method for the *Monument* image is comparable with the ground truth (see Fig. 7). However, ICEVE and BACKLIT suffer from overfitting and merge well- and overexposed regions of the right-sided pillar. In the *Scenery* image (see Fig. 8), only the LNIERD and the proposed method can mark the second brick at the left end corner in the well-exposed zone. Exposure-3R overclassifies the sky region and merges it with the mountain. LEI-ANN and ICEVE have completely misclassified all the bricks into underexposed region. In the *Mountain* image (see Fig. 9), the exposure-3R and BACKLIT method classify many well-exposed regions of mountain and

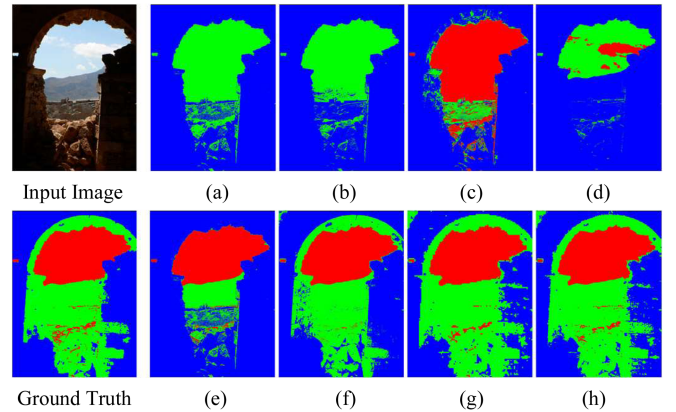


Fig. 8. Visual comparision of the *Scenery* image. The results of different techniques are viz., (a) exposure 2R [8], (b) contrast factor [9], (c) exposure 3R [10], (d) LEI-ANN [36], (e) ICEVE [37], (f) BACKLIT [11], (g) LNIERD [12], and (h) proposed method.

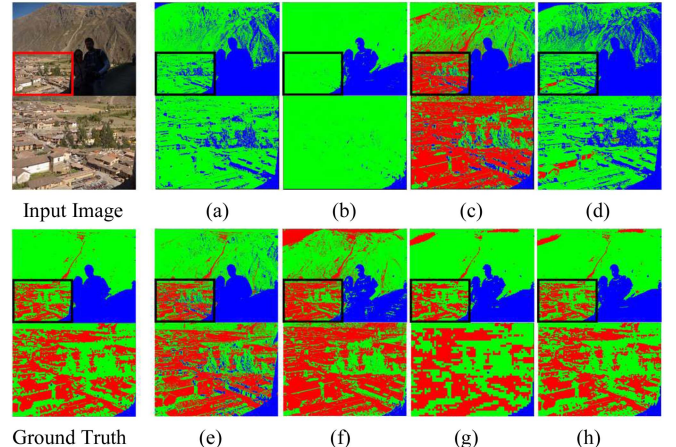


Fig. 9. Visual comparision of the *Mountain* image. The results of different techniques are viz., (a) exposure 2R [8], (b) contrast factor [9], (c) exposure 3R [10], (d) LEI-ANN [36], (e) ICEVE [37], (f) BACKLIT [11], (g) LNIERD [12], and (h) proposed method. For more clear visual analysis, the zoomed portion of the overexposed region of the house is represented in the black box.

cities into overexposed zones. For a more precise analysis, we zoom into the subimage part inside the black box. ICEVE suffers from heavy intertwining of over- and underexposed pixels and LEI-ANN fails to identify the overexposed regions. From the zoomed part, we can also conclude that LNIERD output suffers from the blocking effect, and only the proposed method generates near optimum classification. Finally, we analyze the impact of classification on near-boundary pixels in Fig. 10. The red, black, and yellow boxes represent the area shared by under and well-exposed, well- and overexposed, and all three under-, well-, and overexposed regions, respectively. The exposure-2R, contrast factor, exposure-3R, LEI-ANN, ICEVE, and BACKLIT completely fail to classify the lower half of the *Window* image (red box) into a well-exposed region. The boundary region in the red box is perfectly straight in the LNIERD method, but the same method creates a serious blocking effect in the boundary region, as represented in yellow and black boxes. LEI-ANN, ICEVE, and BACKLIT classify the boundary region perfectly in a yellow box but suffer from overclassification and heavy

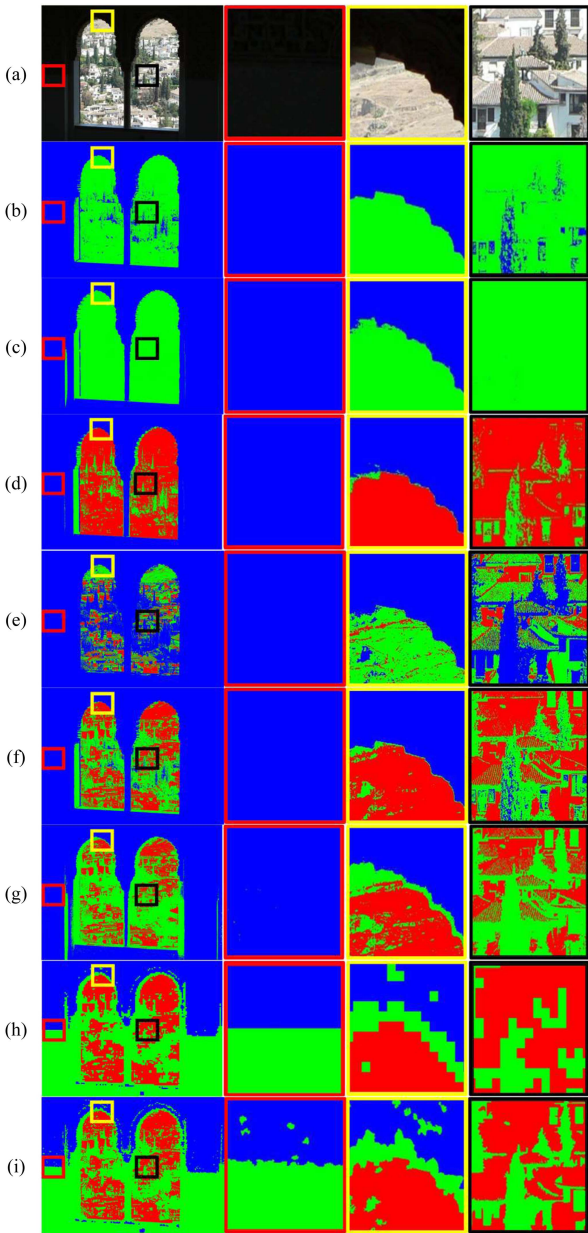


Fig. 10. Visual comparison of the *Window* image. Three different zones are zoomed for boundary pixel analysis. (a) Original image. (b) Exposure 2R [8]. (c) Contrast factor [9]. (d) Exposure 3R [10]. (e) LEI-ANN [36]. (f) ICEVE [37]. (g) BACKLIT [11]. (h) LNIERD [12]. (i) Proposed method.

intertwining in the black box. The proposed method shows the best boundary demarcation in the black box region. However, the proposed method demarcated boundary in the yellow box is slightly distorted but resembles the near-perfect boundary. Apart from a few noisy pixels in the red box, the proposed method signifies the best performance in the overall boundary pixel demarcation.

B. Quantitative Analysis of Classification

Four quantitative parameters are analyzed across the dataset to evaluate the classification performance of the proposed algorithm. The Rand Index (RI) is a similarity function proposed

by William Rand [38], which computes pairwise label relationships. It varies between $[0, 1]$, higher is better. The Variation of Information (VoI) [39] provides information about the average conditional entropy of one classification when the other is established, in our case, the ground truth. It varies between $[0, \infty)$, lower is better. The Global Consistency Error (GCE) represents the extent to which the classification algorithm can be viewed as an alteration of the ground truth. An algorithm with zero GCE signifies the best performance, and one represents the worst [40]. Boundary Displacement Error (BDE) computes average displacement error of boundary pixels between the classified and reference image. It varies between $[0, \infty)$, lower value signifies less amount of error [41]. Tables I and II summarize the performance of algorithms on the five most challenging images. The best value of the corresponding image is represented as bold and the second-best value is represented by an underline. The better performance of the proposed algorithm in terms of RI suggests that the classification result is more correlated with human visual perception. Since we have tried to optimize our entropy, it is not surprising that our algorithm outperforms all other methods by a considerable margin in the VOI index. A minimal value of the GCE parameter suggests a lack of underclassified data in the proposed algorithm output. The BDE indices penalize both undersegmentation and oversegmentation. The low value of the parameter by the proposed method (see Table II) endorses better classification by the algorithm [41]. In each of these images, the proposed method provides the best result for at least three out of four parameters, which signify the robustness of the algorithm toward varying illumination condition. From the box plot (see Fig. 11), it is noteworthy that the proposed method provides minimum variation across different quartiles for all the parameters. It suggests uniform and near-ideal classification performance across various images, taken under different scenarios and conditions. The mean value, median, and quartile distribution for the proposed method are at par compared with these state-of-the-art methods.

IV. APPLICATION OF THE CLASSIFICATION OUTCOME

A novel image enhancement algorithm is also proposed here, which utilizes the outcome of the classification algorithm. We have compared our proposed method with the state-of-the-art enhancement methods, namely DCTSVD [45], DWTSVD [46], ROHIM [47], FCCE [48], LECARM [49], FCBH [50], HMMF [51], and UMGF [52]. We evaluate four highly cited quantitative parameters to analyze the enhancement algorithm, namely entropy [34], FSIM [42], peak signal-to-noise ratio (PSNR) [43], and lightness order error (LOE) [44]. The parameters are chosen such that we can test different aspects of the enhanced images.

A. Proposed Enhancement Algorithm

The proposed enhancement algorithm is applied after converting the image into HSV color space. Since HSV color space separates *luma* or image intensity from *chroma* or color information, thus, the modification of intensity does not impact the color contribution of the overall image. To enhance the underexposed regions, we need to improve their intensity distribution without

TABLE I
RI, VOI, AND GCE VALUES

Image	RI	VOI	GCE
	[8] [9] [10] [36] [37] [11] [12] PRO.	[8] [9] [10] [36] [37] [11] [12] PRO.	[8] [9] [10] [36] [37] [11] [12] PRO.
Scenery	0.67 0.67 0.70 0.65 0.71 0.89 <u>0.90</u> 0.94	1.28 1.22 1.38 1.08 1.14 0.78 <u>0.73</u> 0.49	0.15 0.12 0.22 0.07 0.17 0.14 0.13 <u>0.08</u>
Mountain	0.64 0.82 0.75 0.57 0.86 0.78 <u>0.88</u> 0.94	1.40 <u>0.70</u> 1.22 1.59 0.88 1.10 0.80 0.45	0.26 0.03 0.21 0.34 0.15 0.18 0.14 <u>0.07</u>
Monument	0.83 0.82 <u>0.90</u> 0.61 0.85 0.87 0.90 0.93	0.94 0.96 0.86 1.31 0.93 0.90 <u>0.77</u> 0.46	0.11 <u>0.11</u> 0.15 0.11 0.17 0.18 0.13 0.08
Window	0.64 0.64 0.66 0.62 0.68 0.69 <u>0.87</u> 0.93	1.41 1.47 1.53 1.35 1.41 1.52 <u>0.95</u> 0.45	0.20 0.22 0.26 <u>0.14</u> 0.27 0.33 0.18 0.08
Sea	0.65 0.60 0.68 0.63 0.81 0.90 0.83 <u>0.89</u>	1.47 1.43 1.62 1.64 1.06 <u>0.77</u> 0.97 0.59	0.24 0.18 0.35 0.34 0.21 <u>0.13</u> 0.18 0.11

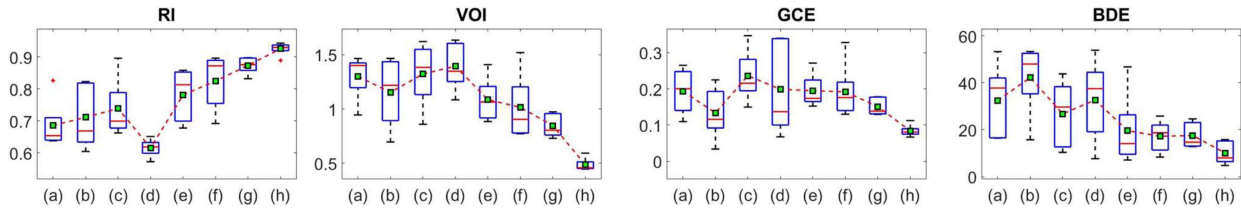


Fig. 11. Statistical comparison of image quality assessment parameters using box plot on all images. Different algorithms used are (a) exposure 2R [8], (b) contrast factor [9], (c) exposure 3R [10], (d) LEI-ANN [36], (e) ICEVE [37], (f) BACKLIT [11], (g) LNIERD [12], and (h) proposed method. The line chart joins the mean value of each algorithm.

TABLE II
BDE VALUES

Image	BDE						
	[8]	[9]	[10]	[36]	[37]	[11]	[12] PRO.
Scenery	53.3	52.3	43.8	53.9	46.8	<u>18.7</u>	22.5 15.8
Mountain	37.8	41.8	29.7	37.5	19.5	25.8 <u>13.1</u> 4.8	
Monument	16.6	15.7	<u>13.5</u>	22.9	10.4	20.7	24.6 15.0
Window	16.4	48.0	10.4	<u>7.7</u>	8.1	12.3	12.8 7.1
Sea	38.3	53.3	36.5	41.3	14.1	<u>8.3</u>	14.7 7.0

impacting the color balance of the whole image. So, we modify the *luma* component using a conceptually designed equation (23)

$$V_O(x, y) = \begin{cases} V_I(x, y) \times \frac{C_u}{\mu_u \times M \times N} & V_I(x, y) \leq \mu_u \\ \frac{C_u}{M \times N} + \frac{V_I(x, y) \times C_w}{\mu_o \times M \times N} & \mu_u < V_I(x, y) \leq \mu_o \\ V_I(x, y) & \mu_o < V_I(x, y) \end{cases} \quad (23)$$

where μ_u and μ_o are the mean values of the intensity of the classified underexposed and overexposed regions. C_u , C_w , and C_o represent the number of underexposed, well-exposed, and overexposed pixels out of the total $M \times N$ pixels of the image. Equation (23), for the underexposed pixels, multiplies the input value of intensity $V_I(x, y)$ by a value greater than “1” obtained as the ratio of distribution density $\frac{C_u}{M \times N}$ and the mean value of the underexposed zone. The range of the obtained intensity $V_O(x, y)$ for the underexposed zone is expanded and, as required, it now occupies a few intensity levels of the well-exposed zone as well. The second section of (23) modifies the intensity distribution of the well-exposed zone. To avoid blocking artifacts, we modify the *luma* component of only those pixels in the well-exposed zone, which have a value near to the pixels of the underexposed zone. We first multiply $V_I(x, y)$ by the ratio of well-exposed region distribution density $\frac{C_w}{M \times N}$ and mean value

of the overexposed region. It is done so that the multiplication factor is less than “1” and pixels do not migrate into the overexposed zone. Then, instead of multiplying here, we shift the input intensity value $V_I(x, y)$ by the ratio of distribution density of underexposed regions $\frac{C_u}{M \times N}$. The *luma* component of the overexposed zone is left untouched by the proposed algorithm.

The very high value of the *luma* component in the overexposed zone overshadows the color characteristics of this zone. Equation (24) alters the saturation value from the HSV color space to produce a visually pleasing image.

$$S_O(x, y)$$

$$= \begin{cases} S_I(x, y) & V_I(x, y) \leq \mu_u \\ \frac{C_u}{M \times N} + \frac{S_I(x, y) \times C_w}{\mu_o \times M \times N} & \mu_u < V_I(x, y) \leq \mu_o \\ \frac{C_w + C_o}{M \times N} (1 - S_I(x, y)) + S_I(x, y) & \mu_o < V_I(x, y). \end{cases} \quad (24)$$

The saturation component $S_I(x, y)$ of the overexposed zone is modified by the third section of (24). It increases the value by adding a term depending on the distribution density of both well- and overexposed regions, namely $\frac{C_w + C_o}{M \times N}$. The factor $(1 - S_I(x, y))$ helps to provide more increment to the pixels with low input saturation value and vice-versa. The saturation of the well-exposed zone is modified similarly as discussed in (23) by replacing the value component with the corresponding saturation component. The *chroma* component of the underexposed zone is left untouched by the proposed algorithm. Finally, the input image, value component modified image, and saturation component modified image are blended using the exposure fusion architecture of the article presented in [53]. The blending of the Laplacian pyramid of the image is done with the Gaussian pyramid decomposed contrast and saturation weights. This helps to avoid any artifact or blocking effects created due to the above changes in under- or overenhanced regions.

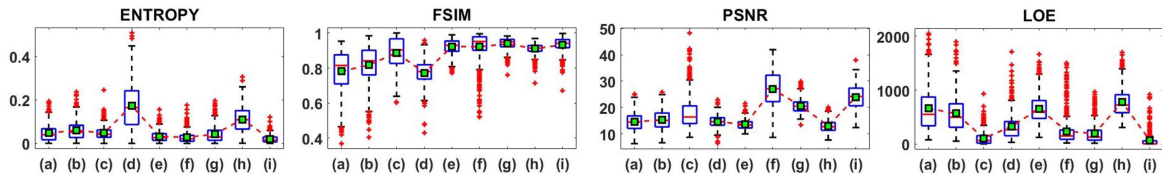


Fig. 12. Statistical comparison of image quality assessment parameters using box plot on all 524 images. Different algorithms used are (a) DCTSVD [45], (b) DWTSVD [46], (c) ROHIM [47], (d) FCCE [48], (e) LECARM [49], (f) FCBH [50], (g) HMMF [51], (h) UMGF [52], and (i) proposed method. The line chart joins the mean value of each algorithm represented by green box.

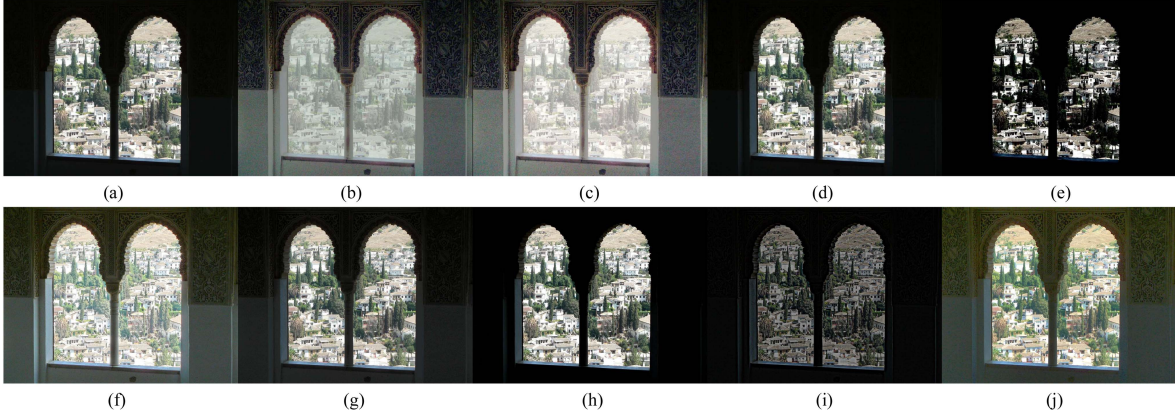


Fig. 13. Visual comparision of *Window* image. (a) Input image and different algorithms used are (b) DCTSVD [45], (c) DWTSVD [46], (d) ROHIM [47], (e) FCCE [48], (f) LECARM [49], (g) FCBH [50], (h) HMMF [51], (i) UMGF [52], and (j) proposed method.

B. Quantitative Analysis

Entropy quantitates the information content of the image. FSIM stands for feature similarity index and encapsulates salient low-level features similarly to human visual system. PSNR informs about the performance of the algorithm in the presence of noise. LOE quantifies the relative lightness order between the enhanced and reference image. An enhanced image tends to have the highest values of FSIM and PSNR and the least value of entropy and LOE parameters. From the box plot in Fig. 12, we can conclude that our method provides the best mean and median values with least number of outliers for entropy, FSIM, and LOE parameters. In terms of performance in the presence of noise, our method gives second-best result for the PSNR value. Very small LOE value symbolizes the naturalness preserving nature of the proposed algorithm. High FSIM value expresses similarity between the enhanced image and human visual system.

C. Visual Analysis

From Fig. 13, one can clearly observe the benefit of the proposed classification algorithm in the task of enhancement. The architecture surrounding the window was completely invisible in the input image. The proper classification of this region as an underexposed area and applying the proposed algorithm bring out the hidden information. Also, due to the reduction of the saturation of the overexposed zone, the modified output scenery appears to be visually pleasing. In comparison with the existing method, we can observe that the outputs of the proposed method, DCTSVD, DWTSVD, and LECARM, are comparable, but the contrast of the proposed method is better. ROHIM, FCCE,

TABLE III
COMPARISON OF THE AVERAGE COMPUTATION TIME USING DIFFERENT ENHANCEMENT METHODS (IN SECONDS)

Image Size	[45]	[46]	[47]	[48]	[49]	[50]	[51]	[52]	Pro.
321 × 481 × 3	1.82	0.28	4.25	0.48	0.09	5.46	0.19	0.11	1.34

UMGF, and HMMF completely fail to demarcate between the architecture and wall boundary. While FCBH fails to enhance the hidden architecture on the window wall. The architectural design on the walls in Fig. 14 is visible only in DCTSVD, DWTSVD enhanced, and proposed method image. However, the latter improves the visual color composition and does not introduce any hazy effect. Fig. 15 signifies the enhancement capability of the proposed algorithm on two more mixed-exposed images.

D. Computation Complexity and Convergence Analysis

Table III summarizes the average computation time on images from BSDS [34] and VV [35] datasets with eight methods, namely DCTSVD [45], DWTSVD [46], ROHIM [47], FCCE [48], LECARM [49], FCBH [50], HMMF [51], and UMGF [52] in MATLAB environment on a laptop, with configuration Intel(R) Core (TM) i7-9850H CPU @ 2.60 GHz, 6 Core(s), 16 GB RAM (CPU). The computation time of the proposed method is much lower than DCTSVD [45], ROHIM [47], and FCBH [50] and is comparable with that of DWTSVD [46] and FCCE [48]. The computation time of the existing methods, such as LECARM [45], HMMF [47], and UMGF [48],

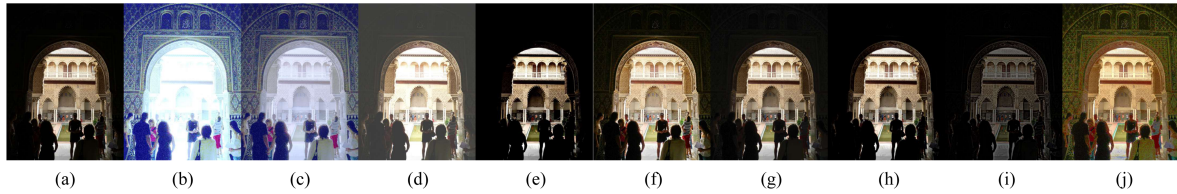


Fig. 14. Visual comparision of *Monument* image. (a) Input image and different algorithms used are (b) DCTSVD [45], (c) DWTSVD [46], (d) ROHIM [47], (e) FCCE [48], (f) LECARM [49], (g) FCBH [50], (h) HMMF [51], (i) UMGF [52], and (j) proposed method.



Fig. 15. (a) Input *Beach* image. (b) Enhanced *Beach* image by the proposed algorithm. (c) Input *Scenery* image. (d) Enhanced *Scenery* image by the proposed algorithm.

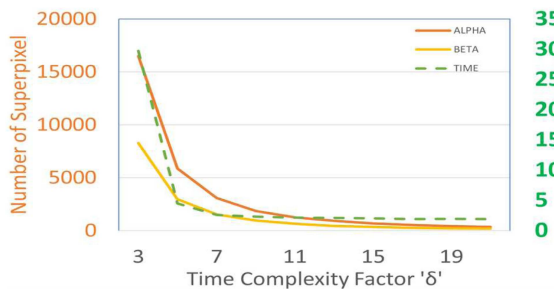


Fig. 16. Convergence curve of the proposed algorithm with respect to time-complexity factor.

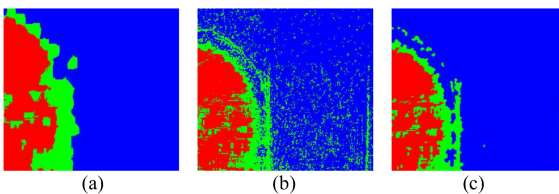


Fig. 17. Impact of the combination of multilevel classification with multi-class SVM. (a) Improper boundary tracing due to small number of superpixel. (b) Overclassification error when large numbers of superpixels are considered. (c) Optimum classified image with the proposed algorithm.

is small; however, the enhanced images from these methods lack clear visual perceptibility. The average time consumed by the proposed algorithm to process an image with the time complexity factor δ equal to 7 is 1.34 s and is comparable with the complexity of the state-of-the-art methods. Fig. 16 represents the convergence curve of the proposed algorithm with respect to the time-complexity factor. When the value of δ is minimum, the number of superpixels α and β is very high and also the computation time is very high. However, such a small value of δ results in overclassification, which, finally, results in lots of noisy pixels [see Fig. 17(b)]. We can also observe that once the value of δ becomes more than 11, both the number of superpixels and computation time converge, and very little

change is observed in their values. A very large value of δ results in a very small number of superpixel with a large size, so it results in improper boundary tracing [see Fig. 17(a)]. Fig. 17 signifies the benefit of the combination of multilevel classification with multiclass SVM. It enables the algorithm to provide proper boundary tracing and avoid overclassification.

V. CONCLUSION

This article proposes a novel multilevel superpixel-based algorithm that trains a multiclass SVM to classify an image into an under-well-over exposed region. The proposed algorithm divides an image into an experimentally determined required number of superpixels. With the help of statistical parameters modeled using Kurtosis of the histogram, a new classification algorithm is proposed, which uses the information from intensity, entropy, and contrast of an image. The multiclass SVM trains itself on different levels of superpixels and provides better results than the state-of-the-art methods by reclassifying the ambiguous regions. We also propose a novel enhancement technique that utilizes the classification result to enhance both saturation and value channel of an HSV image to obtain an enhanced image. Both local and global parameters of the image are enhanced and successfully reinstated to produce perceptually pleasing and informative output. Furthermore, the classification and enhancement algorithm's unparalleled performance is justified by both visual and quantitative analysis. However, the computation time of the proposed algorithm is on higher end due to multilevel classification and multiclass training of SVM. In the future, we will investigate the application of the classification in different fields, such as haze removal and in the field of medical imaging.

REFERENCES

- [1] F. Mendoza and R. Lu, "Basics of image analysis," in *Hyperspectral Imaging Technology in Food and Agriculture*. New York, NY, USA: Springer, 2015, pp. 9–56.
- [2] X. Li, X. Li, Z. Li, X. Xiong, M. O. Khyam, and C. Sun, "Robust vehicle detection in high-resolution aerial images with imbalanced data," *IEEE Trans. Artif. Intell.*, vol. 2, no. 3, pp. 238–250, Jun. 2021.
- [3] W. Liu, X. Shu, L. Zhang, D. Li, and Q. Lv, "Deep multiscale multi-instance networks with regional scoring for mammogram classification," *IEEE Trans. Artif. Intell.*, vol. 3, no. 3, pp. 485–496, Jun. 2022.
- [4] H. Yue, J. Yang, X. Sun, F. Wu, and C. Hou, "Contrast enhancement based on intrinsic image decomposition," *IEEE Trans. Image Process.*, vol. 26, no. 8, pp. 3981–3994, Aug. 2017.
- [5] M. Lecca, "STAR: A segmentation-based approximation of point-based sampling milano retinex for color image enhancement," *IEEE Trans. Image Process.*, vol. 27, no. 12, pp. 5802–5812, Dec. 2018.

- [6] B. Subramani, A. K. Bhandari, and M. Veluchamy, "Optimal Bezier curve modification function for contrast degraded images," *IEEE Trans. Instrum. Meas.*, vol. 70, Apr. 2021, Art. no. 5008910.
- [7] M. Veluchamy, A. K. Bhandari, and B. Subramani, "Optimized Bezier curve based intensity mapping scheme for low light image enhancement," *IEEE Trans. Emerg. Topics Comput. Intell.*, vol. 6, no. 3, pp. 602–612, Jun. 2022.
- [8] M. Hanmandlu, O. P. Verma, N. K. Kumar, and M. Kulkarni, "A novel optimal fuzzy system for color image enhancement using bacterial foraging," *IEEE Trans. Instrum. Meas.*, vol. 58, no. 8, pp. 2867–2879, Aug. 2009.
- [9] K. Hasikin and N. A. M. Isa, "Adaptive fuzzy contrast factor enhancement technique for low contrast and nonuniform illumination images," *Signal, Image Video Process.*, vol. 8, no. 8, pp. 1591–1603, 2014.
- [10] O. P. Verma, P. Kumar, M. Hanmandlu, and S. Chhabra, "High dynamic range optimal fuzzy color image enhancement using artificial ant colony system," *Appl. Soft Comput.*, vol. 12, no. 1, pp. 394–404, 2012.
- [11] S. Lee, N. Kim, and J. Paik, "Adaptively partitioned block-based contrast enhancement and its application to low light-level video surveillance," *SpringerPlus*, vol. 4, 2015, Art. no. 431.
- [12] N. H. Saad, N. A. M. Isa, and A. A. M. Salih, "Local neighbourhood image properties for exposure region determination method in nonuniform illumination images," *IEEE Access*, vol. 8, pp. 79977–79997, 2020.
- [13] N. H. Saad, N. A. M. Isa, and H. M. Saleh, "Nonlinear exposure intensity based modification histogram equalization for non-uniform illumination image enhancement," *IEEE Access*, vol. 9, pp. 93033–93061, 2021.
- [14] S. F. Tan and N. A. M. Isa, "Exposure based multi-histogram equalization contrast enhancement for non-uniform illumination images," *IEEE Access*, vol. 7, pp. 70842–70861, 2019.
- [15] A. Mencattini, M. Salmeri, R. Lojacono, M. Frigerio, and F. Caselli, "Mammographic images enhancement and denoising for breast cancer detection using dyadic wavelet processing," *IEEE Trans. Instrum. Meas.*, vol. 57, no. 7, pp. 1422–1430, Jul. 2008.
- [16] M. Prabukumar, "Compressed domain contrast and brightness improvement algorithm for colour image through contrast measuring and mapping of DWT coefficients," *Int. J. Multimedia Ubiquitous Eng.*, vol. 8, no. 1, pp. 55–70, 2013.
- [17] J. C. Clement and A. Baskar, "Color image enhancement in compressed DCT domain," *ICGST J. Graph., Vis. Image Process.*, vol. 10, no. 1, pp. 31–38, 2010.
- [18] Q. Huang, Z. Miao, S. Zhou, C. Chang, and X. Li, "Dense prediction and local fusion of superpixels: A framework for breast anatomy segmentation in ultrasound image with scarce data," *IEEE Trans. Instrum. Meas.*, vol. 70, Jun. 2021, Art. no. 5011508.
- [19] Z. Zhu, H. Wei, G. Hu, Y. Li, G. Qi, and N. Mazur, "A novel fast single image dehazing algorithm based on artificial multiexposure image fusion," *IEEE Trans. Instrum. Meas.*, vol. 70, 2021, Art. no. 5001523.
- [20] D. Berman, D. Levy, S. Avidan, and T. Treibitz, "Underwater single image color restoration using haze-lines and a new quantitative dataset," *IEEE Trans. Pattern Anal. Mach. Intell.*, vol. 43, no. 8, pp. 2822–2837, Aug. 2021.
- [21] Y. Liu, H. Li, and M. Wang, "Single image dehazing via large sky region segmentation and multiscale opening dark channel model," *IEEE Access*, vol. 5, pp. 8890–8903, 2017.
- [22] L. Wang and H. Wei, "Reconstruction for indoor scenes based on an interpretable inference," *IEEE Trans. Artif. Intell.*, vol. 2, no. 3, pp. 251–259, Jun. 2021.
- [23] B. Arslan, S. Memiş, E. B. Sönmez, and O. Z. Batur, "Fine-grained food classification methods on the UEC food-100 database," *IEEE Trans. Artif. Intell.*, vol. 3, no. 2, pp. 238–243, Apr. 2022.
- [24] P. Shrivakumara, R. P. Sreedhar, T. Q. Phan, S. Lu, and C. L. Tan, "Multioriented video scene text detection through Bayesian classification and boundary growing," *IEEE Trans. Circuits Syst. Video Technol.*, vol. 22, no. 8, pp. 1227–1235, Aug. 2012.
- [25] M. Kumar and A. K. Bhandari, "Contrast enhancement using novel white balancing parameter optimization for perceptually invisible images," *IEEE Trans. Image Process.*, vol. 29, pp. 7525–7536, Jun. 2020.
- [26] M. Kumar and A. K. Bhandari, "No-reference metric optimization-based perceptually invisible image enhancement," *IEEE Trans. Instrum. Meas.*, vol. 71, 2022, Art. no. 5003610.
- [27] R. Achanta, A. Shaji, K. Smith, A. Lucchi, P. Fua, and S. Süsstrunk, "SLIC superpixels compared to state-of-the-art superpixel methods," *IEEE Trans. Pattern Anal. Mach. Intell.*, vol. 34, no. 11, pp. 2274–2282, Nov. 2012.
- [28] R. C. Gonzalez and R. E. Woods, *Digital Image Processing*. London, U.K.: Pearson, 2018.
- [29] C. Wang and Z. Ye, "Brightness preserving histogram equalization with maximum entropy: A variational perspective," *IEEE Trans. Consum. Electron.*, vol. 51, no. 4, pp. 1326–1334, Nov. 2005.
- [30] K. Srinivas, A. K. Bhandari, and A. Singh, "Exposure-based energy curve equalization for enhancement of contrast distorted images," *IEEE Trans. Circuits Syst. Video Technol.*, vol. 30, no. 12, pp. 4663–4675, Dec. 2020.
- [31] P. H. Westfall, "Kurtosis as peakedness, 1905–2014. R.I.P.," *Amer. Statistician*, vol. 68, no. 3, pp. 191–195, 2014.
- [32] T. Joachims, "Making large-scale SVM learning practical," Tech. Univ. Dortmund, Dortmund, Germany, Tech. Rep. 1998,28, 1998.
- [33] L. Wang, P. Xue, and K. L. Chan, "Two criteria for model selection in multiclass support vector machines," *IEEE Trans. Syst., Man, Cybern., B (Cybern.)*, vol. 38, no. 6, pp. 1432–1448, Dec. 2008.
- [34] D. Martin, C. Fowlkes, D. Tal, and J. Malik, "A database of human segmented natural images and its application to evaluating segmentation algorithms and measuring ecological statistics," in *Proc. 8th IEEE Int. Conf. Comput. Vis.*, 2001, pp. 416–423.
- [35] "Busting image enhancement and tone-mapping algorithms: A dataset by Vasileios Vonikakis," 2022. [Online]. Available: <https://sites.google.com/site/vonikakis/datasets>
- [36] M. Kaur and K. Verma, "A novel hybrid technique for low exposure image enhancement using sub-image histogram equalization and artificial neural network," in *Proc. Int. Conf. Inventive Comput. Technol.*, 2016, pp. 1–5.
- [37] C.-H. Lee, L.-H. Chen, and W.-K. Wang, "Image contrast enhancement using classified virtual exposure image fusion," *IEEE Trans. Consum. Electron.*, vol. 58, no. 4, pp. 1253–1261, Nov. 2012.
- [38] P. Arbelaez, M. Maire, C. Fowlkes, and J. Malik, "Contour detection and hierarchical image segmentation," *IEEE Trans. Pattern Anal. Mach. Intell.*, vol. 33, no. 5 pp. 898–916, May 2011.
- [39] C. Pantofaru and M. Hebert, "A comparison of image segmentation algorithms," Carnegie Mellon Univ., Pittsburgh, PA, USA, Tech. Rep. CMU-RI-TR-05-40, 2005.
- [40] M. Meila, "Comparing clusterings: An axiomatic view," in *Proc. 22nd Int. Conf. Mach. Learn.*, 2005, pp. 577–584.
- [41] A. Y. Yang, J. Wright, Y. Ma, and S. S. Sastry, "Unsupervised segmentation of natural images via lossy data compression," *Comput. Vis. Image Understanding*, vol. 110, no. 2, pp. 212–225, 2008.
- [42] L. Zhang, Lei Zhang, X. Mou, and D. Zhang, "FSIM: A feature similarity index for image quality assessment," *IEEE Trans. Image Process.*, vol. 20, no. 8, pp. 2378–2386, Aug. 2011.
- [43] Q. Huynh-Thu and M. Ghanbari, "Scope of validity of PSNR in image/video quality assessment," *Electron. Lett.*, vol. 44, no. 13, pp. 800–801, 2008.
- [44] S. Wang, J. Zheng, H.-M. Hu, and B. Li, "Naturalness preserved enhancement algorithm for non-uniform illumination images," *IEEE Trans. Image Process.*, vol. 22, no. 9, pp. 3538–3548, Sep. 2013.
- [45] A. K. Bhandari, A. Kumar, and P. K. Padhy, "Enhancement of low contrast satellite images using discrete cosine transform and singular value decomposition," *World Acad. Sci., Eng. Technol.*, vol. 79, pp. 35–41, 2011.
- [46] A. K. Bhandari, V. Soni, A. Kumar, and G. K. Singh, "Cuckoo search algorithm based satellite image contrast and brightness enhancement using DWT-SVD," *ISA Trans.*, vol. 53, no. 4, pp. 1286–1296, 2014.
- [47] K. Gu, G. Zhai, W. Lin, and M. Liu, "The analysis of image contrast: From quality assessment to automatic enhancement," *IEEE Trans. Cybern.*, vol. 46, no. 1, pp. 284–297, Jan. 2016.
- [48] A. S. Parihar, O. P. Verma, and C. Khanna, "Fuzzy-contextual contrast enhancement," *IEEE Trans. Image Process.*, vol. 26, no. 4, pp. 1810–1819, Apr. 2017.
- [49] Y. Ren, Z. Ying, T. H. Li, and G. Li, "LECARM: Low-light image enhancement using the camera response model," *IEEE Trans. Circuits Syst. Video Technol.*, vol. 29, no. 4, pp. 968–981, Apr. 2019.
- [50] A. K. Bhandari, S. Shahnawazuddin, and A. K. Meena, "A novel fuzzy clustering-based histogram model for image contrast enhancement," *IEEE Trans. Fuzzy Syst.*, vol. 28, no. 9, pp. 2009–2021, Sep. 2020.
- [51] F. Huo, X. Zhu, H. Zeng, Q. Liu, and J. Qiu, "Fast fusion-based dehazing with histogram modification and improved atmospheric illumination prior," *IEEE Sensors J.*, vol. 21, no. 4, pp. 5259–5270, Feb., 2021.
- [52] Z. Shi, Y. Chen, E. Gavves, P. Mettes, and C. G. M. Snoek, "Unsharp mask guided filtering," *IEEE Trans. Image Process.*, vol. 30, pp. 7472–7485, Aug. 2021.
- [53] T. Mertens, J. Kautz, and F. van Reeth, "Exposure fusion," in *Proc. 15th Pacific Conf. Comput. Graph. Appl.*, Maui, Hawaii, 2007, pp. 382–390.